Ben-Gurion University of the Negev

Faculty of Natural Sciences

Department of Physics

Localized Spatial Structures in Non-Equilibrium Systems

Thesis for the degree

Master of Science

Submitted by: Yair Mau

Advisor: Ehud Meron

January 11, 2009

Localized Spatial Structures in Non-Equilibrium Systems

Thesis for the degree Master of Science

By: Yair Mau
Under the supervision of: Prof. Ehud Meron
Department of Physics
Faculty of Natural Sciences
Ben-Gurion University of the Negev

Signature of the student: _____ Date: _____

Signature of the advisor: _____ Date: _____

Signature of the chairperson of the
committee for graduate studies: _____ Date: _____

Abstract

Localized Spatial Structures in Non-Equilibrium Systems

By: Yair Mau

Thesis for the degree: *Master of Science*

Ben-Gurion University of the Negev, 2009

Symmetry breaking instabilities are often the process by which patterns in nature form. These patterns can be spatially extended or localized. Localized structures have mostly been studied in the context of systems that go through a single pattern forming instability, e.g. dislocation defects in periodic patterns that appear in a Turing instability, or spiral-wave cores in oscillating systems that went through a Hopf bifurcation. A recent study has shown, however, that systems that go through both Hopf and Turing bifurcations can support dual-mode localized structures, e.g. a line defect in a stable Turing pattern that hosts the Hopf mode and gives rise to a breathing defect.

In this thesis we investigate the formation and dynamics of dual-mode localized structures in systems whose equilibrium states go through both a Hopf and a pitchfork bifurcation. We use the normal-form equations for the Hopf-pitchfork bifurcation to study uniform solutions and their stability properties and identify a parameter regime where the pure-Hopf state is the only uniform stable state. In this regime, although the pitchfork mode tends to grow from the unstable equilibrium state, it is nonlinearly damped by the Hopf mode. However, at the cores of spiral-wave solutions, where the nonlinear damping is less effective, the pitchfork mode can potentially grow.

Increasing the distance, ϵ, from the pitchfork bifurcation, we first identify a range where the pitchfork mode is everywhere damped including the spiral core region. Further increase of ϵ, however, leads to an instability of a single-mode spiral wave to a pair of dual-mode spiral waves, where the pitchfork mode is either positive or negative at the spiral core and vanishes away from it. Due to nonlinear coupling between the pitchfork and the Hopf modes, the phase of the Hopf mode is twisted in the core region.

The phase twist induces phase gradients in the radial direction which become steeper as ϵ is increased. Beyond a second threshold these phase gradients induce an oscillatory instability of dual-mode spiral waves, and at yet larger ϵ values spatiotemporal chaos sets in. The latter state is characterized by repeated events of vortex-pair nucleation and annihilation. The general mechanism of these complex dynamical behaviors is spontaneous hosting events of the pitchfork mode in areas of steep gradients of the oscillation phase where the Hopf amplitude is reduced and the nonlinear damping of the pitchfork mode weakens. The spontaneous hosting events induce new phase gradients and the whole process repeats itself a finite number of times in the oscillatory case, and indefinitely in the case of spatiotemporal chaos.

Since the analysis is based on normal form equations the results described above are expected to hold in any system that goes through a Hopf-pitchfork bifurcation. Moreover, we believe that several aspects of our findings, e.g. spontaneous hosting events due to steep phase gradients, can be applicable to other codimension-2 systems such as Hopf-Turing systems.

Acknowledgments

This research project would not have been possible without the support of many people.

First of all, I would like to express my gratitude to my advisor, Prof. Ehud Meron, for his patient guidance, encouragement and excellent advice throughout this research.

Special thanks also to Dr. Aric Hagberg, who received me in Los Alamos, taught me much, and helped me with several issues discussed in this thesis.

I would like to acknowledge our group members, Assaf Kletter and Jonathan Nathan, for their helpful discussions and assistance.

I would like to express my profound gratitude to my beloved family, my parents, my sisters, for always being there for me, for their encouragement and patience.

Finally, I would like to thank from all my heart, my fiancée Liat, for being such a wonderful person, for cheering me up when things didn't go as I expected, and for understanding that moments when I had to turn my attention to the computer and be in another world.

Contents

Chapter 1

Introduction

In nature many far-from-equilibrium systems exhibit instabilities that can induce pattern formation. We loosely define pattern formation as a dynamical process leading to the spontaneous emergence of a nontrivial spatially nonuniform structure which is weakly dependent on initial and boundary conditions. We can understand pattern formation as a process that breaks the symmetry of the system, either in space or in time [1]. These dynamical processes are generally a result of an instability of a stationary homogeneous state, where different kinds of instabilities can yield different kinds of patterns. Finite-wavenumber instabilities produce periodic patterns, either stationary (Turing-like) or traveling. Other instabilities generate either discrete or continuous families of uniform states, which allow spatially structured states. An example of the latter is a Hopf bifurcation to uniform oscillations that allows traveling-wave phenomena when phase gradients are induced. In addition to spatially extended patterns, localized structures often appear: line and point defects in spatially periodic patterns, or vortices in the case of temporal oscillations, form one class of such structures.

Symmetry breaking instabilities leading to pattern formation phenomena have been observed and studied in various systems in many fields of knowledge,

including fluid dynamics, nonlinear optics, granular media, chemical reactions, biology and ecology. These precesses are universal because different systems in nature behave alike when close to the critical point of a same instability.

The localized structures described above involve a single mode, which appears when the equilibrium state loses its stability in a super-critical or sub-critical instability (hereafter the "primary mode"). Driving the system farther away from equilibrium generally leads to a second instability of the equilibrium state, and to the potential growth of a secondary mode. Examples of such situations include Hopf-Turing systems, where the Turing instability is either followed or preceded by a Hopf bifurcation of the same equilibrium state [2], parametric excitation of surface waves, where the growth of one mode is followed by a second mode of different spatial symmetry [3, 4], and other codimension-2 systems. Most studies of codimension-2 systems have focused on mixed-mode states, bistability of pure-mode states, competitive oscillations and chaotic dynamics [2, 5, 6, 7, 8, 9, 10, 11, 12, 13, 14, 15, 16, 17, 18]. However, secondary instabilities of already unstable equilibrium states have received little attention because most often the secondary modes are nonlinearly damped by the primary modes whose amplitudes are much larger. The behavior of a multi-mode system in such situations resembles, in many respects, that of the corresponding single-mode system. For example, a system that goes through both Hopf and Turing bifurcations, but is tuned to the mono-stability range of the Turing mode, shows stationary spatial patterns (e.g. stripes and hexagons) indistinguishable from the patterns produced by a single-mode system that merely goes through a Turing bifurcation. It has recently been demonstrated, however, that the secondary mode can grow in localized structures of the primary mode where its amplitude vanishes or is very small [19], leading to instabilities of single-mode localized structures to dual-mode structures. This phenomenon has been demonstrated in a Hopf-

Turing system where defects in periodic patterns of a dominant Turing mode were found unstable to the local growth of the Hopf mode. The Hopf mode could grow in the defect core because the amplitude of the dominant Turing mode vanishes in this region. The resulting localized structures are more complex as they involve local temporal oscillations. The opposite case of a localized structure of a Hopf mode hosting a Turing mode has also been studied, but only in the context of one-dimensional front structures [19]. In two space dimensions the Hopf mode can form spiral waves. The core of a spiral wave is a two-dimensional localized structure where the Hopf amplitude vanishes. The structure and stability of spiral-wave cores have extensively been studied in the context of single-mode structures [20, 21]; however, multi-mode spiral-core structures have not been studied yet.

Since most studies of codimension-2 systems have focused on dynamical regimes other than secondary instabilities of already unstable equilibrium states, this area still remains propitious for the discovery of new phenomena. The role of the secondary mode in shaping localized structures of the primary mode and in determining their dynamics requires further understanding. In this thesis, we consider the vicinities of a Hopf-pitchfork codimension-2 bifurcation where a Hopf mode nonlinearly damps a pitchfork mode. In the core region of a spiral wave of the Hopf mode, the amplitude of the primary mode goes to zero, and the secondary pitchfork mode is weakly damped. Under these circumstances we expect to find localized structures of the Hopf mode hosting the pitchfork mode. We chose to study this system because it is mathematically simpler than the Hopf-Turing system, and yet may show rich spatio-temporal dynamics.

Chapter 2

Background

2.1 Amplitude Equations

The study of a pattern forming system usually starts with its equations of motion, whose general form (in two space dimensions) can be written as

$$\frac{\partial U}{\partial t} = f\left(U; \partial_x, \partial_y; R\right) , \tag{2.1}$$

where $U = (U_1, U_2, ...)$ is a set of physical variables (temperature, fluid-flow velocities, electric field, chemical concentrations, etc), and f is a nonlinear function of the physical variables U and their spatial derivatives, and of a set of control parameters $R = (R_1, R_2, ...)$. Without loss of generality we can assume that Eq. (2.1) has an equilibrium solution $U = 0$. Quite often such solutions can lose stability to the growth of modes of the form $e^{ikx-i\omega t}$. Four general cases can then be distinguished: (i) $\omega = k = 0$ where the equilibrium solution loses stability to another stationary uniform state(s), (ii) $\omega = 0$, $k \neq 0$, where the instability leads to stationary periodic patterns, (iii) $\omega \neq 0$, $k = 0$, where uniform oscillations set in, and (iv) $\omega \neq 0$, $k \neq 0$, where traveling waves set in.

In general it is not possible to solve analytically the nonlinear equations, but

near an instability point a weak nonlinear analysis can be done. This analysis leads to normal-form or amplitude equations which describe slow modulations in space and in time of a simple pattern solution whose form can be inferred from a linear stability analysis of the equations of motion. The main stages in the derivation of an amplitude equation are sketched below, considering for simplicity a one-dimensional system.

We envisage a system whose equilibrium state $U = 0$ loses stability, as a control parameter R_1 is increased past a critical value R_{1c}, to the growth of a mode of the form $e^{ikx-i\omega t}$. In the vicinity of this instability we can introduce a small parameter $\epsilon = (R_1 - R_{1c})/R_{1c}$. A solution of Eq. (2.1) can then be expressed as power series

$$U(x,t) = \mu_0 U^{(1)} + \mu_0^2 U^{(2)} + \dots , \tag{2.2}$$

where

$$U^{(1)} = A(X,T)e^{ikx-i\omega t} + C.C. , \tag{2.3}$$

μ_0 is a small parameter that scales with ϵ, and $A(X,T)$ is a slowly varying amplitude. The weak dependence of the amplitude on the space and time variables is captured by the introduction of "slow" space $X = \mu_1 x$ and time $T = \mu_2 t$ variables, where μ_1 and μ_2 are other small parameters that scale with ϵ. The manners by which μ_0, μ_1 and μ_2 scale with ϵ depend on the particular equations of motion as discussed below. Note that the derivatives of A with respect to the slow space and time variables are assumed to be of order unity.

The scaling of μ_0 with the distance ϵ to the instability point can often be determined by equating the orders of magnitudes of linear and nonlinear terms. For example, balancing a term ϵU_1 with U_1^3 gives $\mu_0 = \sqrt{\epsilon}$. The scaling of μ_1 with ϵ can be determined by the band width of modes that grow from the equilibrium state when $\epsilon > 0$. For example, a second spatial derivative

(Laplacian) term in a reaction-diffusion system gives a band width that scales like $\sqrt{\epsilon}$ implying $\mu_1 = \sqrt{\epsilon}$. Finally, the scaling of μ_2 with ϵ can be determined from the dependence of the growth rate on ϵ which often leads to $\mu_2 = \epsilon$.

Using the expansion (2.2) in Eq. (2.1) and the following substitutions for the time and space derivatives (using the chain rule),

$$\frac{\partial}{\partial t} \rightarrow \frac{\partial}{\partial t} + \epsilon \frac{\partial}{\partial T} \tag{2.4a}$$

$$\frac{\partial}{\partial x} \rightarrow \frac{\partial}{\partial x} + \sqrt{\epsilon} \frac{\partial}{\partial X}\,, \tag{2.4b}$$

we obtain at any order $\epsilon^{i/2}$ a linear equation for $U^{(i)}$ of the form

$$\mathcal{L} U^{(i)} = R^{(i)}\,, \qquad i = 1, 2, \ldots\,, \tag{2.5}$$

where $\mathcal{L}$ is an operator matrix representing all terms that directly contribute to the i^{th} order, and $R^{(i)}$ represents contributions from lower order terms that are already known at any given order and can be expressed in terms of the amplitude A and its time and spatial derivatives. Equations (2.5) are not always solvable - the right hand side $R^{(i)}$ may contain resonant terms that must be projected out by requiring the right hand side to be orthogonal to the null space of the adjoint of $\mathcal{L}$ with appropriate choice of an inner product (the Fredholm Alternative theorem). These solvability conditions impose constraints on the amplitude A. Once a solvability condition has been imposed at a given order i, the linear equation for $U^{(i)}$ can be solved and used for obtaining the equation for the next order contribution $U^{(i+1)}$. The constraints imposed by the solvability conditions translate into an equation for the amplitude A - the so called "amplitude equation", whereas the calculated contributions $U^{(i)}$ provide an approximate solution to the equations of motion.

The general form of an amplitude equation is determined by the instability

type of the equilibrium state, and is independent of the particular physical system under consideration. This is the reason for the universal nature of pattern formation phenomena - two different physical systems (e.g. a fluid system and a chemical system) that go through the same type of instability will be described close to the instability point by the same amplitude equation and therefore will show similar patterns. The particularity of a system is expressed by the specific forms of the coefficients that appear in the various terms of the amplitude equation.

2.2 Amplitude Equations for Oscillatory Systems

Temporal oscillations in non-equilibrium systems often appear through a Hopf bifurcation to uniform oscillations. This is an instability of an equilibrium state of the 3rd type considered above ($\omega \neq 0$, $k = 0$). The amplitude equation for the Hopf bifurcation (after rescaling the amplitude and time and space coordinates) reads

$$\frac{\partial A}{\partial t} = A - (1 + ic)\,|A|^2\,A + (1 + ib)\nabla^2 A\,, \tag{2.6}$$

where the amplitude A is complex-valued. Equation (2.6) is commonly referred to as the Complex Ginzburg-Landau equation (CGL). The CGL equation is one of the most studied and well understood nonlinear equations in physics [1, 22]. It describes a wide variety of physical phenomena, including nonlinear waves, superconductivity, superfluidity, second-order phase transition, liquid crystals, etc.

The CGL equation has several known solutions in one space dimension (1D) including fronts, pulses, sources and sinks. The latter are spatially localized and represent defects or interfaces that connect domains of regular patterns [23, 24] . In 2D spiral-wave solutions appear. At the center of a spiral wave

the oscillation phase becomes singular. Writing the complex-valued amplitude as $A = \rho e^{i\phi}$, where ρ is the magnitude and ϕ is the phase of oscillations, the following condition holds:

$$\frac{1}{2\pi} \oint_C \vec{\nabla}\phi \cdot \vec{dl} = 1\,, \tag{2.7}$$

where C is any closed contour containing the spiral center. This condition implies a phase singularity because it holds also for arbitrarily small contours. The amplitude A can remain non-singular only if ρ vanishes at the spiral core as figure 2.1 shows.

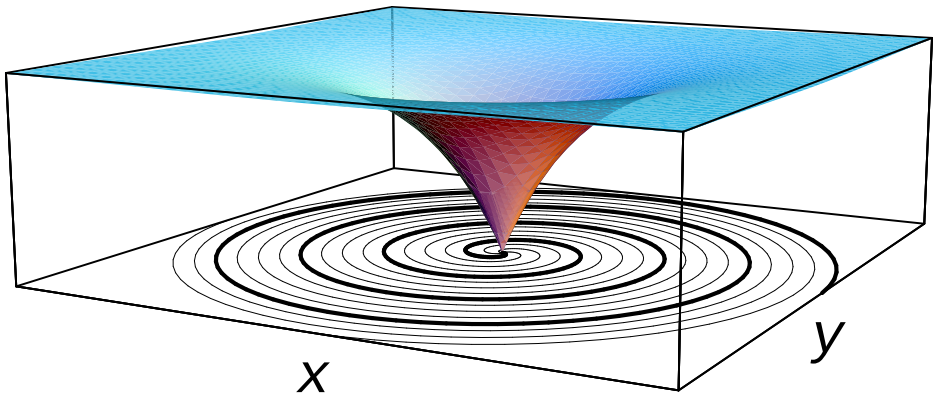

Figure 2.1: The core of a spiral wave as a localized structure. The height of the surface indicates the magnitude ρ, and the spiraling curves are isophase lines (the phase change between two thin lines is $\pi/2$). Figure reprinted with permission of [25], copyright 1997 by the American Physical Society.

As will be shown in Chapter 4, the core of the spiral, which is the region where the magnitude ρ deviates significantly from its asymptotic value, provides a suitable example for studying hosting phenomena of secondary modes.

Chapter 3

The Model Equations

In this thesis we will study systems that undergo both Hopf and pitchfork bifurcations. We conceive a physical system that has a control parameter R_1, and as it is increased the system is driven away from equilibrium. The equilibrium state loses stability at R_{1a} to the growth of a Hopf mode, and at $R_{1b} > R_{1a}$ to the growth of a pitchfork mode. We assume that the system has another control parameter R_2, and when it reaches a critical value R_{2c} the two instabilities merge in a codimension-2 point. That is, at $R_2 = R_{2c}$, $R_{1a}(R_{2c}) = R_{1b}(R_{2c})$ holds, and both the Hopf and pitchfork modes grow simultaneously. In the vicinity of the codimension-2 point we can approximate a typical dynamical variable of the system as

$$u = c_1 A e^{i\omega_H t} + c_2 v + C.C. + \dots , \tag{3.1}$$

where c_1 and c_2 are constants, ω_H is the Hopf frequency, and $C.C.$ stands for complex conjugate. Substituting this ansatz in the equations that describe the system and using multiple time scales analysis will give us amplitude equations for A and v of the form

$$A_t = (\mu + i\nu)A - (\beta_1 + i\beta_2)|A|^2 A + (\alpha_1 + i\alpha_2)\nabla^2 A$$
$$- (\Gamma_1 + i\Gamma_2)Av - (\Delta_1 + i\Delta_2)Av^2 \tag{3.2a}$$
$$v_t = \Lambda + Ev - \kappa v^3 + D\nabla^2 v$$
$$+ \Sigma|A|^2 - H|A|^2 v\,, \tag{3.2b}$$

where we have assumed that the coefficients β_i, α_i, κ and D are all positive.

The first line of equation (3.2a) constitutes the well know complex Ginzburg-Landau equation [22], where μ is the distance from the Hopf bifurcation and ν is the deviation from the Hopf frequency ω_H. The first line of equation (3.2b) constitutes the cusp bifurcation equation with a diffusion term, where Λ is responsible for the imperfection of the pitchfork bifurcation and E is the cusp bifurcation parameter. The terms in the second line of each equation are resonant terms that couple these two equations. These equations represent the normal-form equations of a Hopf-cusp bifurcation [26].

We can rescale equations (3.2) by making the following substitutions, assuming $\mu > 0$:

$$A = \sqrt{\frac{\mu}{\beta_1}} A' e^{i\frac{\nu t}{\mu}}\ ;\quad v = \sqrt{\frac{\mu}{\kappa}} v'\ ;\quad t = \frac{1}{\mu} t'\ ;\quad x = \sqrt{\frac{\alpha_1}{\mu}} x' \tag{3.3}$$

Equations (3.2) then become, after dropping the primes for simplicity,

$$A_t = A - (1 + i\beta)|A|^2 A + (1 + i\alpha)\nabla^2 A$$
$$- (\gamma_1 + i\gamma_2)Av - (\delta_1 + i\delta_2)Av^2 \tag{3.4a}$$
$$v_t = \lambda + \epsilon v - v^3 + d\nabla^2 v + \sigma|A|^2 - \eta|A|^2 v\,, \tag{3.4b}$$

where

$$\beta = \frac{\beta_2}{\beta_1}\,; \quad \alpha = \frac{\alpha_2}{\alpha_1}\,; \quad \gamma_1 = \frac{\Gamma_1}{\sqrt{\mu\kappa}}\,; \quad \gamma_2 = \frac{\Gamma_2}{\sqrt{\mu\kappa}}\,; \quad \delta_1 = \frac{\Delta_1}{\kappa}\,; \quad \delta_2 = \frac{\Delta_2}{\kappa}\,;$$
$$\lambda = \Lambda\sqrt{\frac{\kappa}{\mu^3}}\,; \quad \epsilon = \frac{E}{\mu}\,; \quad d = \frac{D}{\alpha_1}\,; \quad \sigma = \frac{\Sigma}{\beta_1}\sqrt{\frac{\kappa}{\mu}}\,; \quad \eta = \frac{H}{\beta_1}\,. \tag{3.5}$$

By rescaling the amplitude of A we were able to eliminate β_1, and by rescaling the phase of A we were able to go to the rotating frame of the system, and thus eliminating ν. The rescaling of v, t and x enabled us to get rid of κ, μ and α_1, respectively.

In this thesis we will work with a simplified version of these equations, obtained by setting $\lambda = \sigma = 0$. The equations then represent a Hopf-pitchfork bifurcation. To better understand the role of each parameter, we can substitute $A = \rho e^{i\phi}$ into equation (3.4), and get (with $\lambda = \sigma = 0$):

$$\rho_t = \rho\left(1 - \rho^2 - \gamma_1 v - \delta_1 v^2\right) + \nabla^2\rho - \rho(\nabla\phi)^2 - 2\alpha\nabla\rho\nabla\phi - \alpha\rho\nabla^2\phi \tag{3.6a}$$

$$\phi_t = -\beta\rho^2 - \gamma_2 v - \delta_2 v^2 + \nabla^2\phi + \tfrac{2}{\rho}\nabla\rho\nabla\phi + \tfrac{\alpha}{\rho}\nabla^2\rho - \alpha(\nabla\phi)^2 \tag{3.6b}$$

$$v_t = v\left(\epsilon - v^2 - \eta\rho^2\right) + d\nabla^2 v\,. \tag{3.6c}$$

Note that equations (3.6) are invariant under the phase shift transformation $A \to Ae^{i\phi_0}$; $v \to v$, where ϕ_0 is an arbitrary constant.

In the next chapter we will study uniform stationary solutions of (3.6) and their stability to homogeneous and non-homogeneous perturbations.

Chapter 4

Uniform Solutions and their Stability Properties

4.1 Spatially Homogeneous Perturbations

We first study the stability of uniform solutions of equations (3.6) to homogeneous perturbations. Taking the spatial derivatives equal to zero, we get the following ODEs:

$$\rho_t = \rho\left(1 - \rho^2 - \gamma_1 v - \delta_1 v^2\right) \tag{4.1a}$$

$$\phi_t = -\beta\rho^2 - \gamma_2 v - \delta_2 v^2 \tag{4.1b}$$

$$v_t = v\left(\epsilon - v^2 - \eta\rho^2\right) . \tag{4.1c}$$

Note that the equation for the phase ϕ is decoupled from the equation for ρ and v. We can therefore study equations (4.1a) and (4.1c) independently of (4.1b), find their stationary solutions $(\rho_\star, v_\star)$, and analyse their stability properties. The phase equation can then be integrated to give $\phi(t) = \omega t + \phi_0$, where $\omega = -\beta\rho_\star^2 - \gamma_2 v_\star + \delta_2 v_\star^2$, and ϕ_0 is an arbitrary constant. There are

four types of stationary solutions $(\rho_\star, v_\star)$: $(0,0)$ is called the zero-state; $(0, v_0)$ represents a pure pitchfork state; $(\rho_0, 0)$ represents a pure Hopf state; and (ρ_m, v_m) represents a mixed state involving both the Hopf and the pitchfork modes.

We study the linear stability of a solution $(\rho_\star, v_\star)$ inserting the form

$$\begin{pmatrix} \rho \\ v \end{pmatrix} = \begin{pmatrix} \rho_\star \\ v_\star \end{pmatrix} + \begin{pmatrix} \delta\rho \\ \delta v \end{pmatrix} e^{\xi t} \tag{4.2}$$

into equations (4.1), assuming $\delta\rho$ and δv to be infinesimally small. This leads to

$$\det \begin{pmatrix} 1 - 3\rho_\star^2 - \gamma_1 v_\star - \delta_1 v_\star^2 - \xi & -\gamma_1\rho_\star - 2\delta_1\rho_\star v_\star \\ -2\eta\rho_\star v_\star & \epsilon - 3v_\star^2 - \eta\rho_\star^2 - \xi \end{pmatrix} = 0\,, \tag{4.3}$$

and solving the determinant above will give the characteristic equation for the eigenvalues. The static solution will be stable only if both eigenvalues are negative, otherwise the solution is unstable to homogeneous perturbations.

We will now study the stability of each of the four solutions separately, considering two interesting simplifications of the system.

4.1.1 Parameters $\gamma_1 \neq 0$, $\delta_1 = 0$

In this case the characteristic equation for the eigenvalues ξ_i reads

$$\left(1 - 3\rho_\star^2 - \gamma_1 v_\star - \xi\right)\left(\epsilon - 3v_\star^2 - \eta\rho_\star^2 - \xi\right) - 2\eta\gamma_1\rho_\star^2 v_\star = 0 \tag{4.4}$$

and the stability properties of the four types of solution are as described bellow:

(a1) $(\boldsymbol{\rho_\star = 0, v_\star = 0})$

Solving (4.4) for $(\rho_\star = 0, v_\star = 0)$ we find $\xi_1 = 1$ and $\xi_2 = \epsilon$; therefore,

this solution is always unstable.

(b1) $(\boldsymbol{\rho_\star = 0, v_\star = v_0})$

To find the value of v_0 we take equations (4.1) with $\rho = 0$. The result is $v_0 = \pm\sqrt{\epsilon}$. Solving (4.4) for $(\rho_\star = 0, v_\star = \pm\sqrt{\epsilon})$, we find $\xi_1 = 1 \mp \gamma_1\sqrt{\epsilon}$ and $\xi_2 = -2\epsilon$. For $\epsilon > 0$, ξ_2 is always negative. The solution $(\rho_\star = 0, v_\star = \pm\sqrt{\epsilon})$ will be stable for $\xi_1 < 0$, i.e., when $1 < \pm\gamma_1\sqrt{\epsilon}$. For positive values of γ_1, the upper branch of the pitchfork will be stable for $\epsilon > \frac{1}{\gamma_1^2}$, and the lower branch of the pitchfork will always be unstable.

(c1) $(\boldsymbol{\rho_\star = \rho_0, v_\star = 0})$

To find the value of ρ_0 we take equations (4.1) with $v = 0$. The result is $\rho = 1$. Solving (4.4) for $(\rho_\star = 1, v_\star = 0)$ we find $\xi_1 = -2$ and $\xi_2 = \epsilon - \eta$. The eigenvalue ξ_1 is always negative, and the solution $(\rho_\star = 1, v_\star = 0)$ will be stable for $\epsilon < \eta$.

(d1) $(\boldsymbol{\rho_\star = \rho_m, v_\star = v_m})$

To find the values of ρ_m and v_m we solve the system of equations (4.1), and the solution is:

$$\rho_m^{\pm} = \sqrt{1 - \frac{\gamma_1}{2}\left(\eta\gamma_1 \pm \sqrt{\eta^2\gamma_1 - 4(\eta - \epsilon)}\right)} \tag{4.5a}$$

$$v_m^{\pm} = \frac{1}{2}\left(\eta\gamma_1 \pm \sqrt{\eta^2\gamma_1^2 - 4(\eta - \epsilon)}\right) \tag{4.5b}$$

The $+(-)$ sign denotes that the pitchfork mode is in its upper (lower) branch. These solutions are limited to a region of the parameter space where $\eta^2\gamma_1^2 - 4(\eta - \epsilon) > 0$, i.e., to $\epsilon > \eta - \frac{1}{4}\eta^2\gamma_1^2$. The stability analysis of this state is straightforward but tedious, and the stability criteria are too long to display.

4.1.2 Parameters $\gamma_1 = 0,\ \delta_1 \neq 0$

In this case the characteristic equation is

$$\left(1 - 3\rho_\star^2 - \delta_1 v_\star^2 - \xi\right)\left(\epsilon - 3v_\star^2 - \eta\rho_\star^2 - \xi\right) - 4\delta_1\eta\rho_\star^2 v_\star^2 = 0 \tag{4.6}$$

and the stability properties are as follows:

(a2) $(\boldsymbol{\rho_\star = 0, v_\star = 0})$

Solving (4.6) for $(\rho_\star = 0, v_\star = 0)$ we find $\xi_1 = 1$ and $\xi_2 = \epsilon$, therefore this solution is always unstable.

(b2) $(\boldsymbol{\rho_\star = 0, v_\star = v_0})$

To find the value of v_0 we take equations (4.1) with $\rho = 0$. The result is $v_0 = \pm\sqrt{\epsilon}$. Solving (4.6) for $(\rho_\star = 0, v_\star = \pm\sqrt{\epsilon})$ we find $\xi_1 = 1 - \delta_1\epsilon$ and $\xi_2 = -2\epsilon$. For $\epsilon > 0$, ξ_2 is always negative. The solution $(\rho_\star = 0, v_\star = \pm\sqrt{\epsilon})$ will be stable for $\xi_1 < 0$, i.e., when $\epsilon > \frac{1}{\delta_1}$.

(c2) $(\boldsymbol{\rho_\star = \rho_0, v_\star = 0})$

To find the value of ρ_0 we take equations (4.1) with $v = 0$. The result is $\rho = 1$. Solving (4.6) for $(\rho_\star = 1, v_\star = 0)$ we find $\xi_1 = -2$ and $\xi_2 = \epsilon - \eta$. The eigenvalue ξ_1 is always negative, and the solution $(\rho_\star = 1, v_\star = 0)$ will be stable for $\epsilon < \eta$.

(d2) $(\boldsymbol{\rho_\star = \rho_m, v_\star = v_m})$

To find the values of ρ_m and v_m we solve the system of equations (4.1), and solution is:

$$\rho_m = \sqrt{\frac{\delta_1\epsilon - 1}{\eta\delta_1 - 1}} \tag{4.7a}$$

$$v_m^{\pm} = \pm\sqrt{\frac{\eta - \epsilon}{\eta\delta_1 - 1}} \tag{4.7b}$$

The $+(-)$ sign denotes that the pitchfork mode is in its upper (lower) branch. These solutions are limited to $\frac{1}{\delta_1} < \epsilon < \eta$ for $\eta\delta_1 > 1$ and $\eta < \epsilon < \frac{1}{\delta_1}$ for $\eta\delta_1 < 1$. Solving (4.6) for $(\rho_\star = \rho_m, v_\star = v_m^\pm)$ we find that the mixed mode is stable for $\eta\delta_1 < 1$ and unstable for $\eta\delta_1 > 1$. In the latter case there is a bistability range of the two pure-mode states. Figure 4.1 shows bifurcation diagrams for both cases.

4.2 Spatially Periodic Perturbations

In section 4.1 have analysed the stability of four uniform solutions of (3.6) to homogeneous perturbations. Since in this thesis we are interested in situations where the Hopf mode dominates the pitchfork mode, we concentrate on parameter ranges where the pure-Hopf state is stable. Below we show that whenever this state is stable to uniform perturbations, it is also stable to non-uniform perturbations. We consider the Hopf-pitchfork amplitude equations

$$\begin{aligned} A_t = A - (1+i\beta)|A|^2A + (1+i\alpha)\nabla^2 A \\ - (\gamma_1 + i\gamma_2)Av - (\delta_1 + i\delta_2)Av^2 \qquad (4.8a) \\ v_t = \epsilon v - v^3 + d\nabla^2 v - \eta|A|^2 v\,, \qquad (4.8b) \end{aligned}$$

and pure-Hopf uniform solutions $A_0 = \rho_0 e^{i\omega t + \phi_0}$, $v_0 = 0$, where ρ_0 and ϕ_0 are constants. Substituting A_0 and v_0 into (4.8) we get $\rho_0 = 1$ and $\omega = -\beta$. The constant ϕ_0 is an arbitrary phase which we set to zero. We study the stability of this solution using the following form of non-uniform perturbations:

$$A = e^{-i\beta t}(1 + a_+ e^{i\vec{q}\cdot\vec{x}} + a_-^\star e^{-i\vec{q}\cdot\vec{x}}) \tag{4.9a}$$

$$v = V(e^{i\vec{q}\cdot\vec{x}} + e^{-i\vec{q}\cdot\vec{x}})\,. \tag{4.9b}$$

Inserting this form into equations (4.8) we find after projecting onto $e^{\pm i\vec{q}\cdot\vec{x}}$:

$$\dot{a}_+ = \left[-1 - i\beta - q^2(1 + i\alpha)\right] a_+ - (1 + i\beta)a_- - (\gamma_1 + i\gamma_2)V \tag{4.10a}$$

$$\dot{a}_- = -(1 + i\beta)a_+ + \left[-1 - i\beta - q^2(1 + i\alpha)\right] a_- - (\gamma_1 + i\gamma_2)V \tag{4.10b}$$

$$\dot{V} = (\epsilon - \eta - dq^2)V\,. \tag{4.10c}$$

Inserting now

$$\begin{pmatrix} a_+ \\ a_- \\ V \end{pmatrix} = \begin{pmatrix} a_+^0 \\ a_-^0 \\ V^0 \end{pmatrix} e^{\xi t} \tag{4.11}$$

in equations (4.10) we find the following characteristic equation for the eigenvalues ξ:

$$(\epsilon - \eta - dq^2 - \xi)\left[\left(-1 - i\beta - q^2(1 + i\alpha) - \xi\right)^2 - (1 + i\beta)^2\right] = 0\,. \tag{4.12}$$

The solutions are

$$\xi_1 = \epsilon - \eta - dq^2$$
$$\xi_2 = -2 - q^2 - i(2\beta + q^2\alpha)$$
$$\xi_3 = -q^2 - iq^2\alpha\,.$$

These results are consistent with the results we have found in section 4.1, meaning that spatial periodic perturbations do not change the stability conditions of the pure-Hopf state when comparing to homogeneous perturbations.

Had we considered traveling-wave solutions of equations (4.8), $A_0 = \rho_0 e^{ikx \pm i\omega t}$, we would have found the usual Eckhaus and zigzag instabilities to longitudinal and transverse perturbations, respectively.

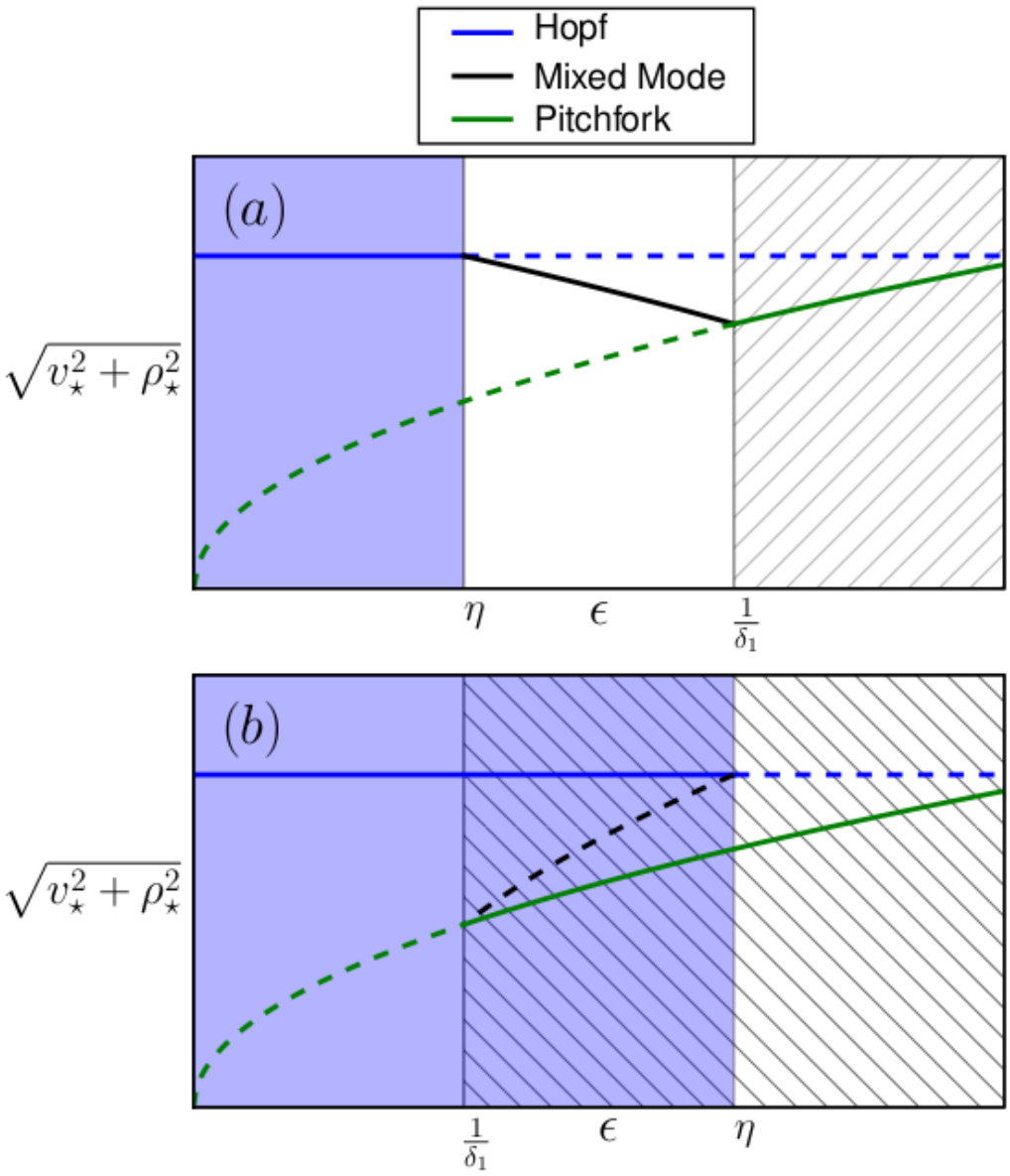

Figure 4.1: Bifurcation diagrams showing stationary uniform solutions of equations (4.1) and their stability properties. Solid (dashed) lines represent stable (unstable) solutions. Blue, green and black lines denote pure-Hopf, pure-pitchfork and mixed-mode states, respectively. In (a) $\eta\delta_1 < 1$ and the mixed-mode is stable. In (b) $\eta\delta_1 > 1$ and the mixed mode is unstable. In this case there is a bistability range of the two pure-mode states.

Chapter 5

Dual-mode Localized Structures

A well studied nonuniform solution of the CGL equation is the spiral wave [22, 27]. The core of a spiral wave is a localized structure where the oscillations amplitude goes to zero [25]. As we have seen in subsection 4.1.2 the pure pitchfork state is unstable for $\epsilon < \eta$, i.e., in the region of stable pure Hopf state. This happens because of the term $-\eta\rho^2$ in equation (3.6c), which nonlinearly damps the pitchfork mode by effectively changing the pitchfork bifurcation point from zero to $\epsilon_{bp} = \eta\rho^2$. This displacement of the bifurcation point depends on the magnitude ρ, so we expect to see that effect to be weaker in the center of a spiral wave, where $\rho \to 0$. We may therefore expect to find an instability of a single-mode spiral wave, involving the Hopf mode only, to a dual-mode spiral wave involving both the hosting Hopf mode and the hosted pitchfork mode at the spiral core.

The appearance of the pitchfork mode v at the spiral core will accelerate or decelerate the oscillation phase there. This becomes evident by looking at the term $-\gamma_2 v$ in equation (3.6b); for $\gamma_2 > 0$, when v is in the upper (lower) branch of the pitchfork it will decelerate (accelerate) the phase. The local phase change at the core region creates phase gradients in the radial direction since the phase remains unaffected away from the core region. These gradients

reduce the oscillations magnitude ρ and may lead to additional hosting events and rich spatio-temporal dynamics as discussed in the following sections.

We will consider a system in a stable pure Hopf state and study first the destabilization of single-mode spiral wave to a dual-mode spiral wave. We will then study secondary instabilities of dual-mode spiral waves as we keep increasing the distance from the pitchfork bifurcation.

5.1 An instability of a Single-Mode Spiral Wave

Integrating numerically Eqs. (4.8) above the pitchfork bifurcation point, $\epsilon > 0$, we first find an ϵ range where single-mode spiral waves are still stable, despite the fact that the hopf-mode amplitude vanishes at the spiral core and is less effective in damping the pitchfork mode v. However, as ϵ exceeds a critical value, ϵ_c, the single-mode spiral-wave solution loses stability to a pair of dual-mode spiral wave solutions, where v is no longer zero at the spiral core and assumes either positive or negative values as the bifurcation diagram in Fig. 5.1 shows.

Figure 5.2 shows the two-dimensional distributions of the v field and of the Hopf phase, $\phi = \arg A$ below (a,b) and above (c,d) the spiral-wave instability. The v field acts to twist the Hopf phase in the spiral-core region, clockwise or counter-clockwise, leaving it unchanged away from the core. This effect (induced by the term $-\gamma_2 v$ in equation (3.6)) creates a phase gradient in the radial direction.

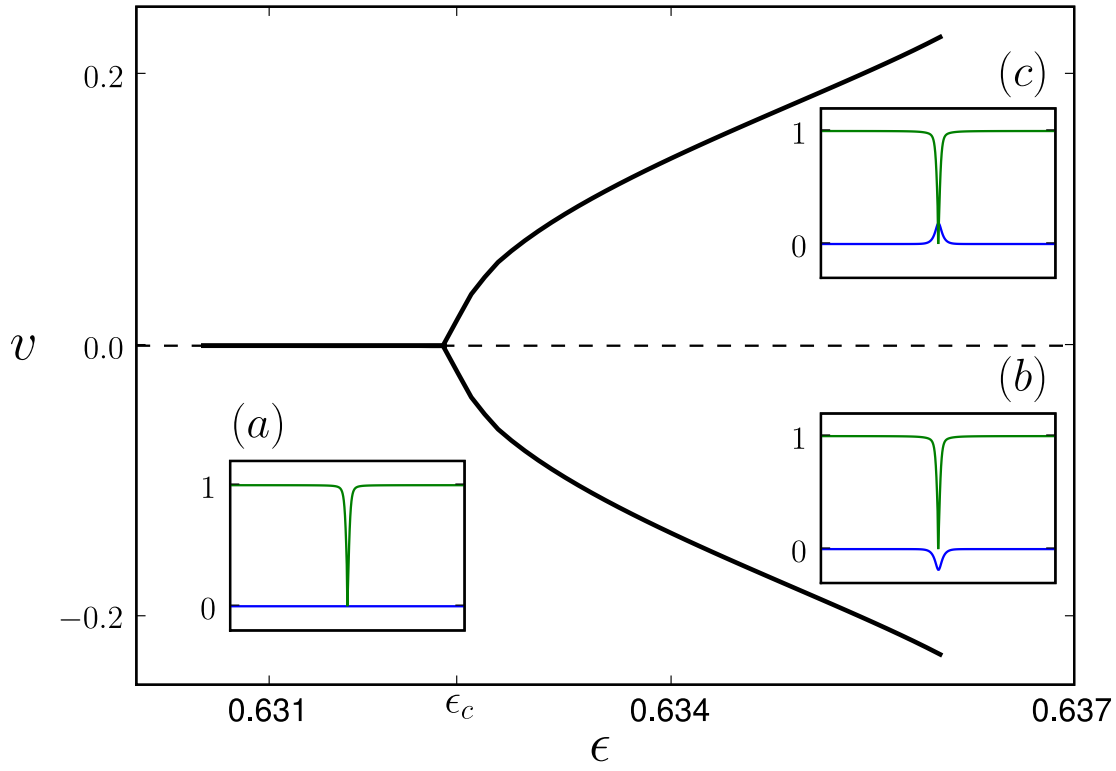

Figure 5.1: Bifurcation diagram showing the instability of a single-mode spiral wave to a pair of dual mode spiral waves. The diagram depicts the value of v at the spiral center as a function of the distance from the pitchfork bifurcation ϵ. The insets show the magnitude ρ of the Hopf amplitude and the v field along a cut through the spiral centers: below the instability ($\epsilon = 0.62$) the v field is zero everywhere (a), while above the instability ($\epsilon = 0.635$) the v field is either negative (b) or positive (c) at the spiral core. The green line represents ρ and the blue line v. Parameters: $\gamma_2 = 1$, $\delta_1 = 0.8$, $d = 1$, $\eta = 0.8$, and all the other parameters are zero. For these parameter values $\epsilon_c = 0.6324$.

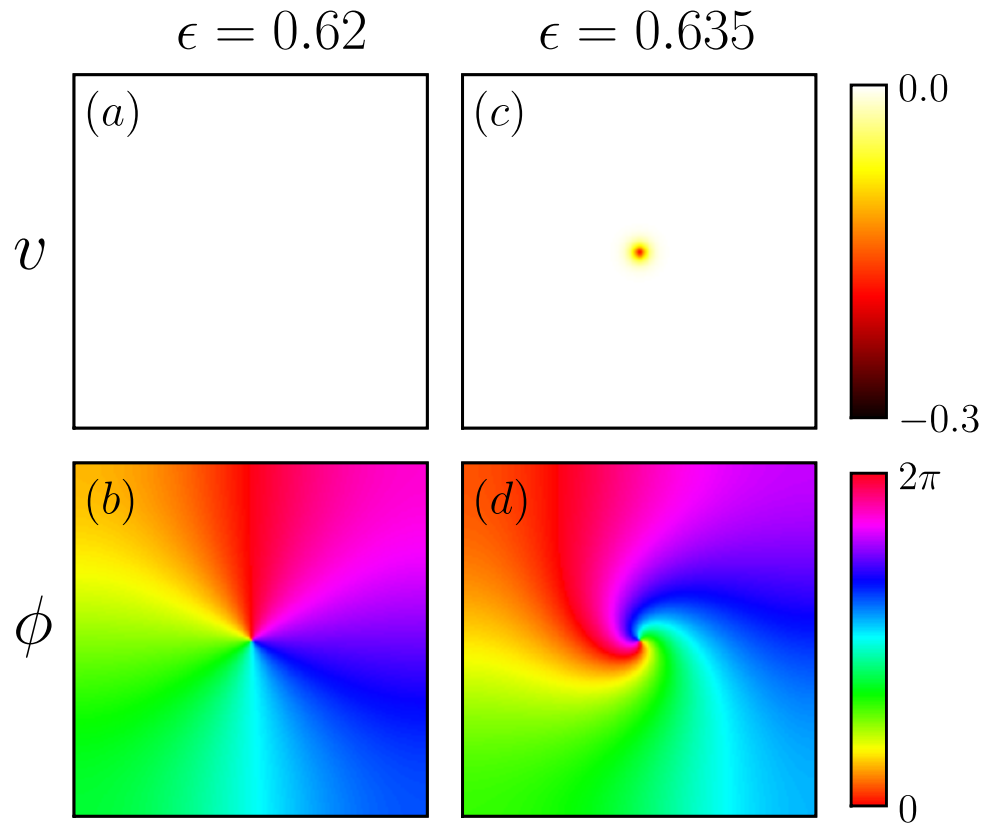

Figure 5.2: The phase-twist effect of the v field beyond the instability to dual-mode spiral waves. Below the instability, where $v = 0$ everywhere (a), equal-phase lines are radial, reflecting no dependence of the phase $\phi = \arg A$ on the distance from the spiral core (b). Beyond the instability equal-phase lines are twisted by the v field at the spiral core, giving rise to phase gradients in the radial direction. Parameters: $\epsilon = 0.62$ (a,b) $\epsilon = 0.635$ (c,d), $\gamma_2 = 1$, $\delta_1 = 0.8$, $d = 1$, $\eta = 0.8$, and all the other parameters are zero.

5.2 Oscillatory Instability of a Dual-Mode Spiral Wave

As ϵ is increased beyond the instability threshold, ϵ_c, to dual-mode spiral waves, a second threshold is found where the static dual-mode spiral core loses stability to a pulsating spiral core as Fig. 5.3 shows. For the parameters used the instability is subcritical.

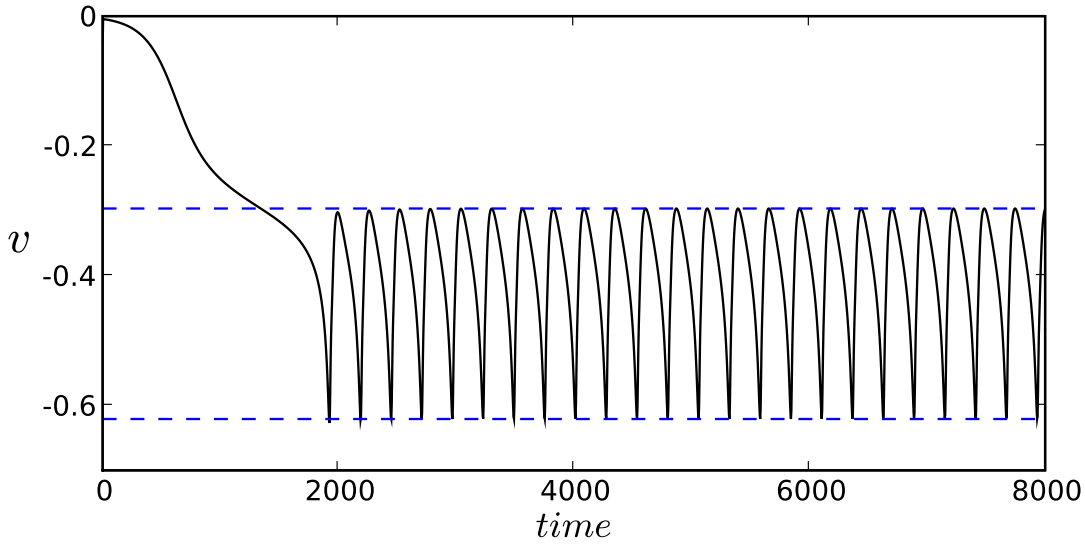

Figure 5.3: Periodic oscillations of a dual-mode spiral core. Shown is the value of v at the spiral center as a function of time. Parameters: $\gamma_2 = 1$, $\delta_1 = 0.8$, $\epsilon = 0.638$, $d = 1$, $\eta = 0.8$, and all the other parameters are zero.

Figure 5.4 shows the three fields v ρ and ϕ along a cycle of the periodic dynamics. Also shown are cuts of v, ρ and $|\nabla\phi|^2$ across the spiral center. The snapshots show three hosting events of the v field at increasing distances from the spiral center. To understand these processes we rewrite the model

equations in terms of the phase gradient $K = \nabla\phi$. The equations now read

$$\rho_t = \rho\left(1 - \rho^2 - \delta_1 v^2 - (K)^2\right) + \nabla^2\rho \tag{5.1a}$$

$$K_t = -\gamma_2\nabla v - \frac{2}{\rho}\left[\frac{1}{\rho}(\nabla\rho)^2 - \nabla^2\rho\right]K + \frac{2}{\rho}\nabla\rho\nabla K + \nabla^2 K \tag{5.1b}$$

$$v_t = v\left(\epsilon - v^2 - \eta\rho^2\right) + d\nabla^2 v \tag{5.1c}$$

The equations do not contain terms whose coefficients have been set to zero in the numerical investigations. The local build up of the v field at the spiral core (for $\epsilon > \epsilon_c$), where the Hopf amplitude vanishes, creates a negative gradient of v in the radial direction. According to Eq. (5.1b) this gradient creates a phase gradient K. This gradient, in turn, decreases the Hopf amplitude (see Eq. (5.1a)). If the buildup of v at the spiral core is strong enough, this process can induce a second hosting event in which the v field builds up in a circle around the spiral center where the Hopf amplitude is small (second snapshot from top in Fig. 5.4. The second hosting event moves the region of highest gradient of v further away from the spiral center and a similar process can take place again leading to another hosting event at a yet larger circle around the spiral center (third snapshot from top in Fig. 5.4). When the gradient of v (away from the spiral center) becomes too weak no further hosting events take place and a new cycle begins.

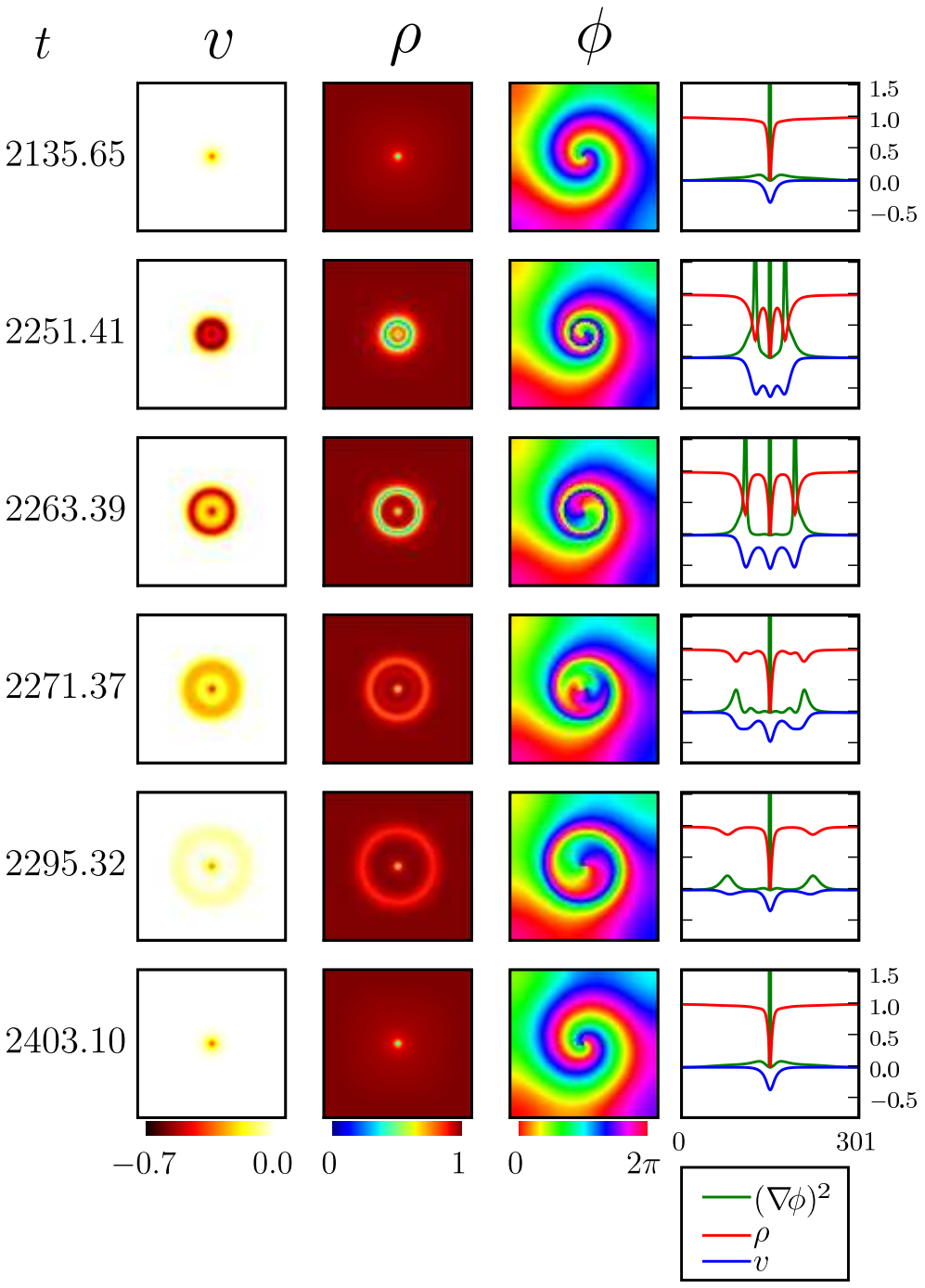

Figure 5.4: Spiral-core oscillations as a result of successive hosting events. Shown are the v, ρ and ϕ fields along one period of oscillations. Also shown are cuts of v, ρ and $|\nabla\phi|^2$ across the spiral center. For more details see the text. Parameter values are the same as in Fig. 5.3.

5.3 Transition to Spatio-Temporal Chaos

For sufficiently higher values of ϵ the series of hosting events at larger and larger distances from the spiral center do not stop and an irregular state eventually develops as Fig. 5.5 shows. The irregular dynamics at the spiral center is demonstrated by the time signal shown in Fig. 5.6. The irregular asymptotic state is characterized by repeated events of vortex-pair nucleation and annihilation, typical of other realizations of spatio-temporal chaos [28, 29, 30, 31]. The number of vortices fluctuates as Fig. 5.7 shows but the mean number does not decay, reflecting a statistical steady state in which the rate of vortex-pair nucleation equals the rate of annihilation. Vortex-pair nucleation results from spontaneous hosting events occurring along line segments where steep gradients of the oscillation phase develop, as the right column in Fig. 5.8 shows. Along these segments the magnitude ρ of the Hopf amplitude reduces to small values that allow hosting of the pitchfork mode v. To the best of our knowledge, this is a new mechanism of spatio-temporal chaos in extended dissipative systems. We note that since $\alpha = \beta = 0$ in our simulations, the condition $1 + \alpha\beta < 0$ for Benjamin-Feir turbulence is not satisfied.

An interesting aspect of this state of spatio-temporal chaos is that it coexists with stable pure-Hopf oscillations in which the Hopf amplitude is bounded away from zero. Chaotic oscillations set in only when the Hopf amplitude becomes small enough to allow for hosting of the pitchfork mode, as is the case with a spiral vortex as an initial condition. The bistability of chaotic and regular states is demonstrated in Fig. 5.9. Shown is a chaotic state invading the regular state. Regular-state regions far from the interface remain stable to vortex nucleation, but when the interface reaches the boundaries the whole system oscillates chaotically. The coexistence of a stable regular state suggests however that the chaotic state is not truly asymptotic as there might be a

rare event where all vortices annihilate one another (or their images in the boundaries). Once such an event occurs there is no driving force for hosting events and the system is expected to settle at the stable pure-Hopf state from which it cannot escape anymore. The pure-Hopf state in this context plays a role similar to an "absorbing state" in nonequilibrium phase-transitions [32].

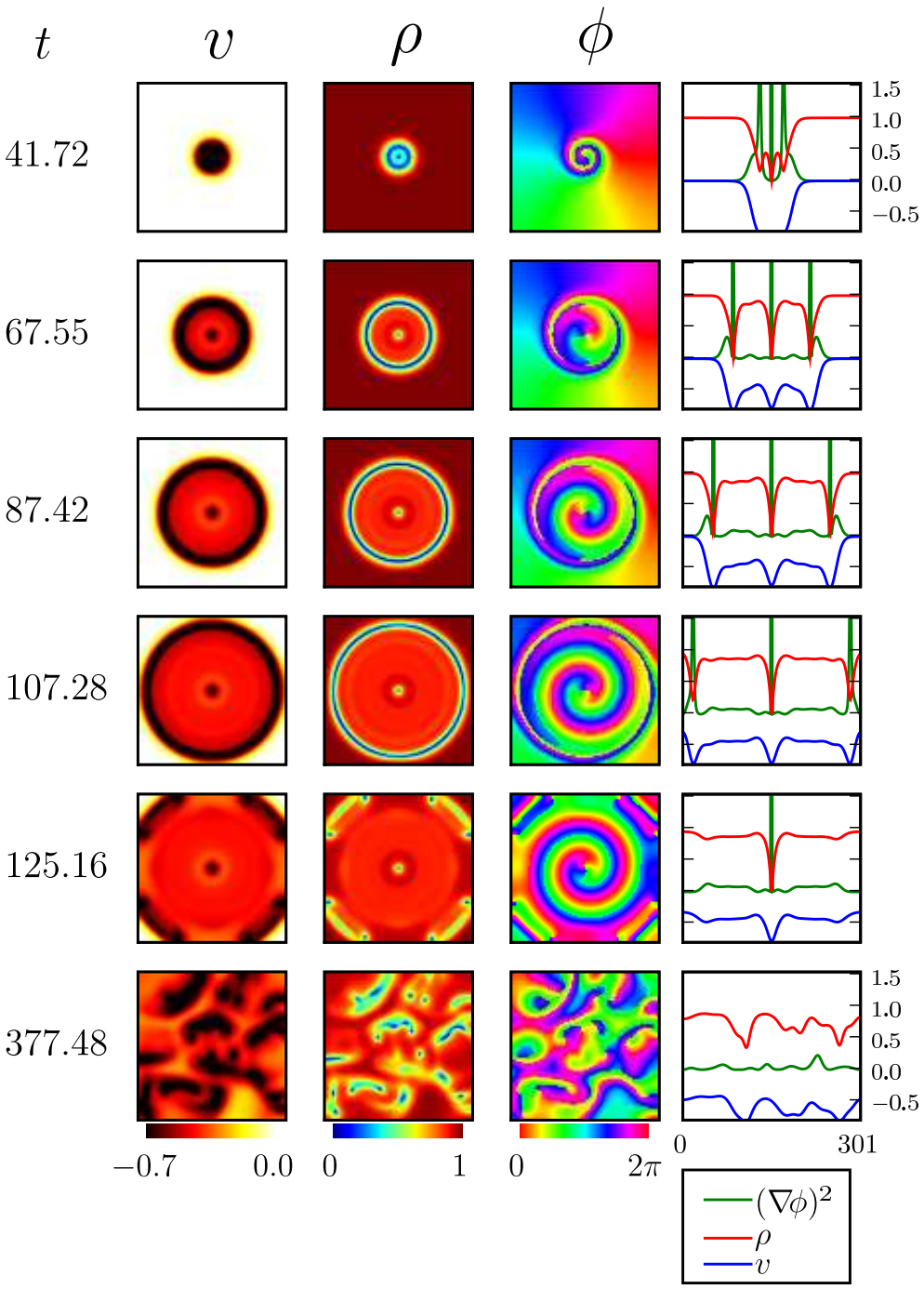

Figure 5.5: Spatio-temporal chaos induced by spiral-core instability. Shown are the fields v, ρ and ϕ along a series of hosting events that eventually reach the system boundaries (dark circles of the v field), and in the asymptotic chaotic state. Also shown are the corresponding cuts of v, ρ and $|\nabla\phi|^2$ across the spiral center. Parameters are as in Fig. 5.6.

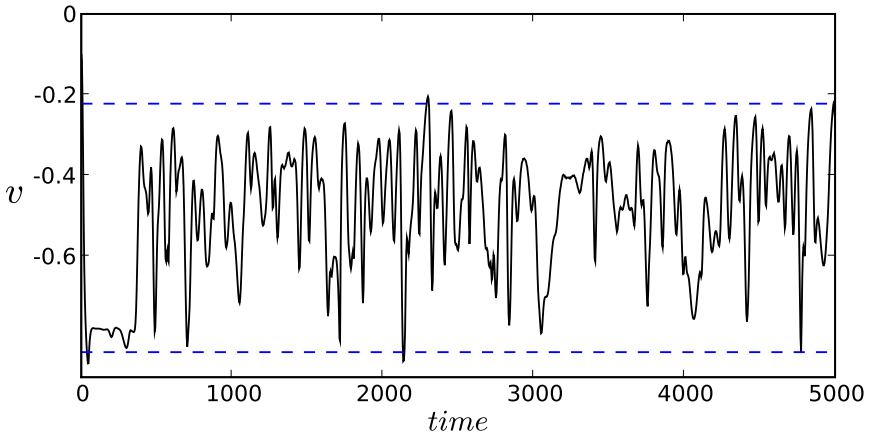

Figure 5.6: Irregular dynamics of a dual-mode spiral core. Shown is the value of v at the spiral center as a function of time. Parameters: $\gamma_2 = 1$, $\delta_1 = 0.8$, $\epsilon = 0.8$, $d = 1$, $\eta = 0.8$, and all the other parameters are zero.

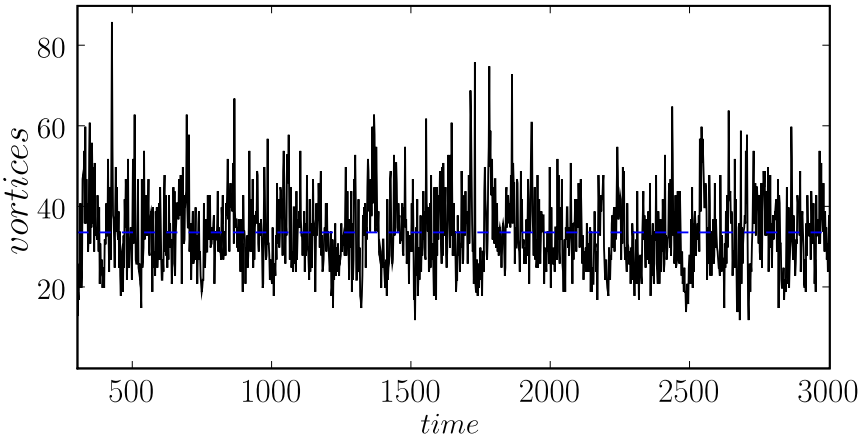

Figure 5.7: Fluctuations of the number of vortices in time. The dashed line indicates the mean vortex number. The methods used to identify and count the vortices are explained in subsections 5.4.3 and 5.4.4. Parameters are as in Fig. 5.6.

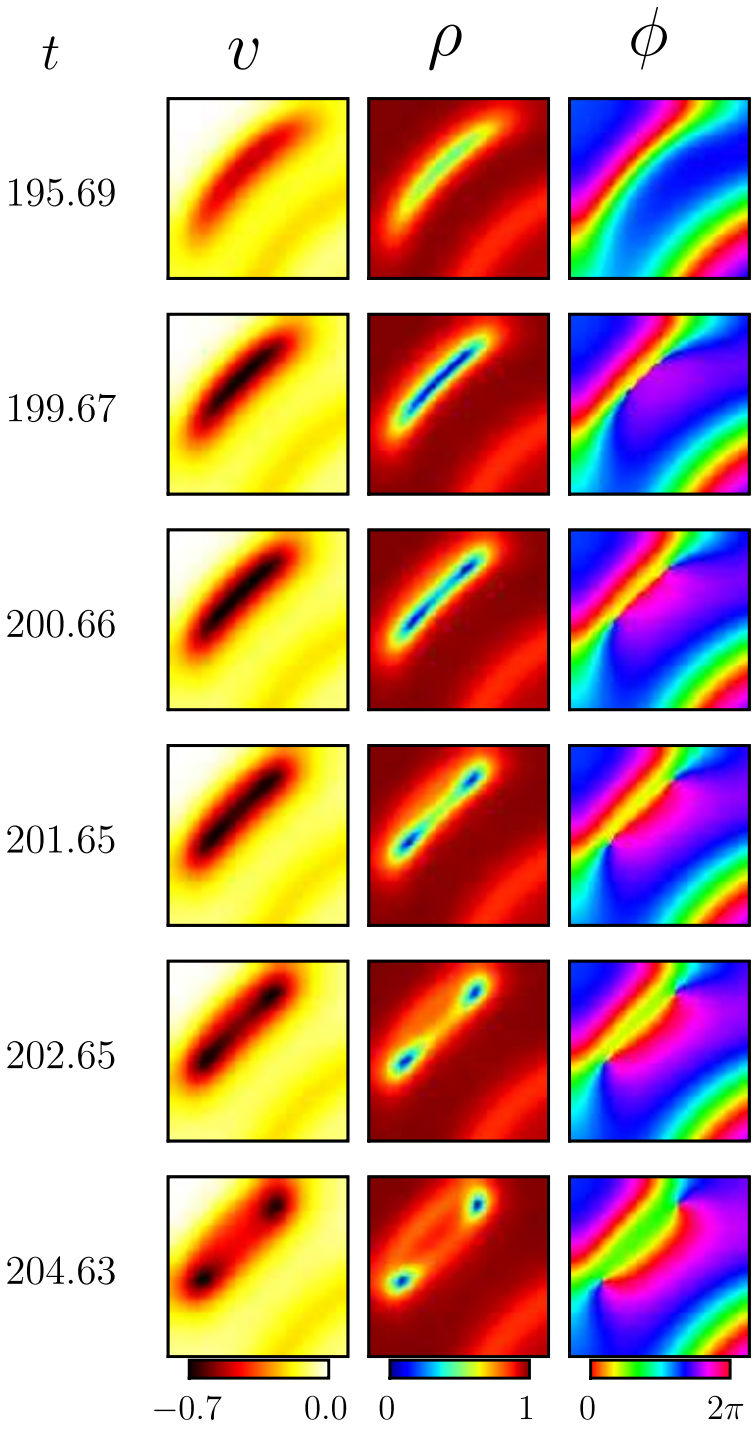

Figure 5.8: The nucleation of a vortex pair from a hosting event occurring along a line segment where the phase gradient becomes steep and the Hopf amplitude reduces significantly. Parameters are as in Fig. 5.6, except for $\epsilon = 0.7$.

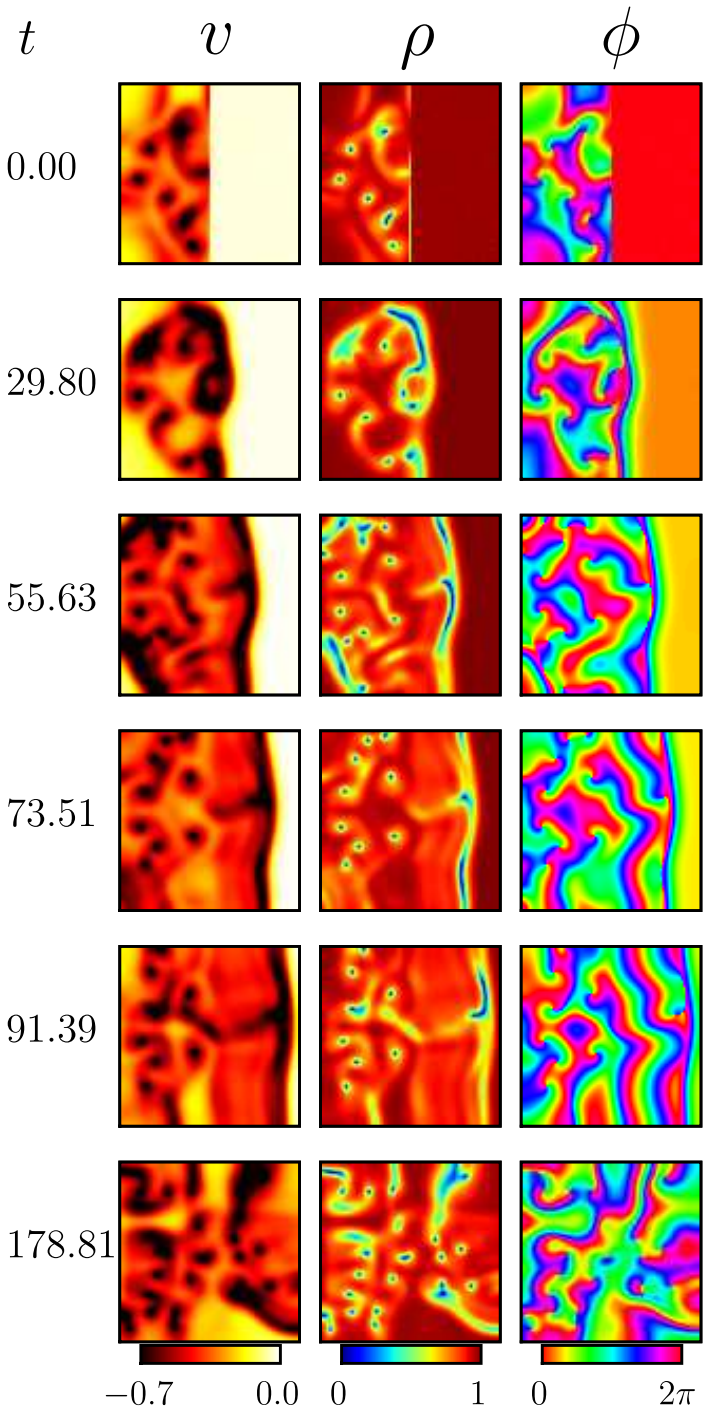

Figure 5.9: A state of spatio-temporal chaos invading a pure-Hopf state. The initial conditions for this simulation consist of a domain of spatio-temporal chaos (left half) and a domain of pure Hopf oscillations (right half). As time proceeds a front structure develops at the interface between the two domains. The front propagates to the right until the chaotic state occupies the whole system. Parameters are as in Fig. 5.6, except for $\epsilon = 0.78$.

5.4 Numerical Methods

5.4.1 Initial and Boundary Conditions

In order to get single or dual-mode spiral wave solutions whose cores lie at the system center, we used the following initial conditions: $\rho = 1$ everywhere, $\phi = \theta$, where θ is the angle of polar coordinates, and a Gaussian form for v whose extremum point lies at the system's center. In all simulations we used Neumann boundary conditions, i.e., $\nabla A = 0$ and $\nabla v = 0$ at the borders.

5.4.2 Finite Differences

The simulations in this work were carried out using codes written in C and Python. We used the method of finite differences combined with Euler method for the time integration. The Laplacian operator was calculated using a 5-point stencil method [33] in the following way:

$$\nabla^2 u \longrightarrow \nabla^2 u_{i,j} = \frac{u_{i+1,j} + u_{i-1,j} + u_{i,j+1} + u_{i,j-1} - 4u_{i,j}}{h^2} \tag{5.2}$$

where i, j is the position of the point on the grid and h is the grid spacing.

5.4.3 Identifying a Vortex

We identify a vortex within a closed contour line C using the condition

$$\oint_C \vec{\nabla}\phi \cdot \vec{dl} = 2\pi \,. \tag{5.3}$$

We calculate this condition using the following four-point sum:

$$\oint_C \vec{\nabla}\phi \cdot \vec{dl} \longrightarrow \sum_{i=1}^{4} \frac{\phi_{i+1} - \phi_i}{h} (dl)_{i,i+1} \tag{5.4}$$

where ϕ_i denotes the value of ϕ at the ith grid point, and the index i runs in a cyclic manner along points that form the smallest square on the grid as illustrated in Fig. 5.10. The value of $(dl)_{i,i-1}$ can be either h or $-h$.

According to Fig. 5.10 the sum can be explicitly written as

$$\frac{\phi_2-\phi_1}{h}(h)+\frac{\phi_3-\phi_2}{h}(h)+\frac{\phi_4-\phi_3}{h}(-h)+\frac{\phi_1-\phi_4}{h}(-h)=2(\phi_3-\phi_1)\,. \quad (5.5)$$

Equation (5.5) means that in order to calculate the closed integral, we just have to evaluate the phase difference between any two diagonal points in the smallest square we can draw on the grid. If we are to find a vortex inside this square the difference should be $2|\phi_3-\phi_1|\simeq 2\pi$. Thus, the test we employ in order to identify vortices is to check whether $|\phi_c-\phi_a|\simeq\pi$.

5.4.4 Calculating the Number of Vortices

We calculate the number of vortices in a chaotic state using the phase singularity test $|\phi_1-\phi_3|\simeq\pi$. Any pair of grid points (e.g. 1 and 3) whose phases differ by approximately π should necessarily belong to non-adjacent quadrants of the complex A plane as illustrated in Fig. 5.11. Such pairs of grid points satisfy $Re(A_{i,j})\cdot Re(A_{i+1,j+1})<0$ *and* $Im(A_{i,j})\cdot Im(A_{i+1,j+1})<0$. To calculate the number of vortices on a $L\times L$ grid, we create a $(L-1)^2$ matrix with all its entries zero, representing a plane with no vortices. Then we assign the value 1 to every matrix element (i,j) where both conditions $Re(A_{i,j})\cdot Re(A_{i+1,j+1})<0$ and $Im(A_{i,j})\cdot Im(A_{i+1,j+1})<0$ are satisfied. Summing over all matrix elements we obtain the total number of vortices.

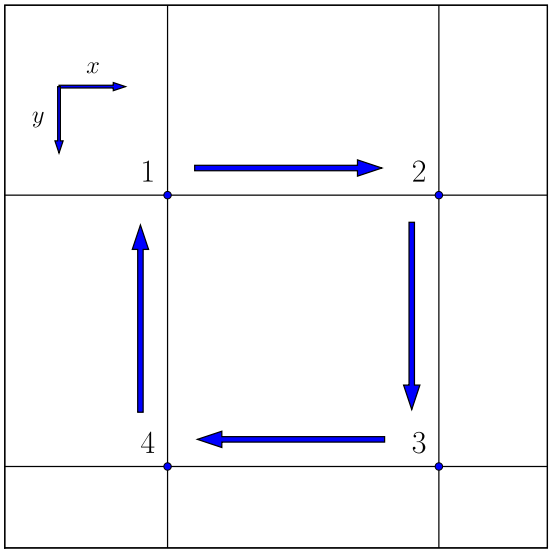

Figure 5.10: The cyclic sequence of grid points along which the phase singularity condition (5.3) or the sum (5.5) is calculated.

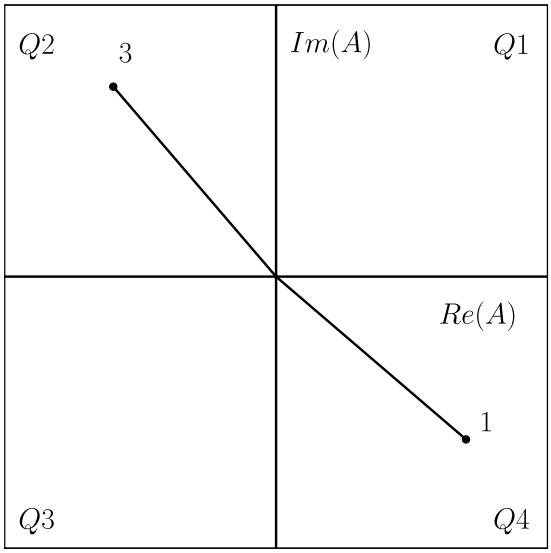

Figure 5.11: Locations of grid points 1 and 3 in non-adjacent quadrants of the complex A plane as a criterion for the existence of a vortex. The labels Qi denotes the ith quadrant.

Chapter 6

Conclusion

We have studied here the formation and destabilization of dual-mode spiral waves in oscillatory Hopf systems whose core regions host a pitchfork mode. The effect of the hosted pitchfork mode v is to twist the oscillation phase and induce phase gradients in the radial direction (Fig. 5.2). These phase gradients have the potential of destabilizing the dual-mode spiral waves, because such gradients reduce the oscillation amplitude $|A|$ and form conditions that favor further hosting events of the pitchfork mode.

Indeed, increasing the distance ϵ from the pitchfork bifurcation, which results in steeper phase gradients, leads to the destabilization of a static dual-mode spiral wave to an oscillatory dual-mode spiral wave. Each oscillation cycle consists of a series of hosting events at increasing radii (Fig. 5.4). At yet higher ϵ values, when the circles reach the system's boundaries a state of spatiotemporal chaos develops (Fig. 5.5). This state is characterized by the spontaneous nucleation of spiral vortex pairs along line segments where the Hopf amplitude is sufficiently reduced to allow for hosting of the pitchfork mode (Fig. 5.8). After a transient period a statistical steady state seems to appear in which vortex pairs repeatedly nucleate and annihilate, but keep the total vortex number fluctuating about a constant mean value (Fig. 5.7). Since

this chaotic state coexists with a linearly stable Pure-hopf state (with $v = 0$ everywhere), rare events leading to the collapse of the chaotic state to the absorbing pure-Hopf state, cannot be excluded.

To the best of our knowledge, this is a new mechanism of spatio-temporal chaos that may possibly appear in codimension-2 systems other than Hopf-pitchfork, e.g. in Hopf-Turing systems. We have demonstrated it numerically but detailed mathematical analysis is needed in order to further clarify the spontaneous hosting events that destabilize dual-mode spiral waves, as well as vortex-pair nucleation processes.

Hosting phenomena at the cores of spiral waves and the possible destabilization of the resulting dual-mode spirals to a state of spatio-temporal chaos, can possibly be tested in experiments on chemical reactions. One candidate for such reactions is the chlorine dioxide-iodine malonic acid (CDIMA) reaction [34] which exhibits Hopf and Turing bifurcations along with a wide range of pattern formation phenomena. Another candidate reaction is the Belousov-Zhabotinsky (BZ) reaction dispersed in a water-in-oil aerosol OT (AOT) microemulsion (BZ-AOT) [35, 36]. This system, too, exhibits a rich spatio-temporal dynamics, including Turing structures and oscillatory patterns [37].

Bibliography

[1] M. C. Cross and P. C. Hohenberg. Pattern formation outside of equilibrium. *Reviews of Modern Physics*, 65:851–1112, 1993.

[2] E Dulos, J Boissonade, JJ Perraud, B Rudovics, and P DeKepper. Chemical morphogenesis: Turing patterns in an experimental chemical system. *Acta Biotheoretica*, 44(3-4):249–261, NOV 1996.

[3] S Ciliberto and JP Gollub. Pattern Competition Leads To Chaos. *Physical Review Letters*, 52(11):922–925, 1984.

[4] H Arbell and J Fineberg. Spatial and temporal dynamics of two interacting modes in parametrically driven surface waves. *Physical Review Letters*, 81(20):4384–4387, 1998.

[5] Ingo Rehberg and Guenter Ahlers. Experimental observation of a codimension-two bifurcation in a binary fluid mixture. *Phys. Rev. Lett.*, 55(5):500–503, Jul 1985.

[6] J.-J. Perraud, A. De Wit, E. Dulos, P. De Kepper, G. Dewel, and P. Borckmans. One-dimensional "spirals": Novel asynchronous chemical wave sources. *Phys. Rev. Lett.*, 71(8):1272–1275, Aug 1993.

[7] Barbara J. A. Zielinska, David Mukamel, Victor Steinberg, and Shmuel Fishman. Phase diagram of externally modulated Rayleigh-Bénard system

near the codimension-two point. *Phys. Rev. A*, 34(5):4171–4180, Nov 1986.

[8] P. Kolodner. Coexisting traveling waves and steady rolls in binary-fluid convection. *Physical Review E*, 48:R665–R668, August 1993.

[9] A. De Wit, G. Dewel, and P. Borckmans. Chaotic Turing-Hopf mixed mode. *Phys. Rev. E*, 48(6):R4191–R4194, Dec 1993.

[10] A. de Wit, D. Lima, G. Dewel, and P. Borckmans. Spatiotemporal dynamics near a codimension-two point. *Physical Review E*, 54:261–271, July 1996.

[11] M. Meixner, S. Bose, and E. Schöll. Analysis of complex and chaotic patterns near a codimension-2 Turing-Hopf point in a reaction-diffusion model. *Phys. D*, 109(1-2):128–138, 1997.

[12] M. Meixner, A. de Wit, S. Bose, and E. Schöautll. Generic spatiotemporal dynamics near codimension-two Turing-Hopf bifurcations. *Physical Review E*, 55:6690–6697, June 1997.

[13] M. Tlidi, Paul Mandel, and M. Haelterman. Spatiotemporal patterns and localized structures in nonlinear optics. *Phys. Rev. E*, 56(6):6524–6530, Dec 1997.

[14] Tlidi M. and Haelterman M. Robust Hopf-Turing mixed-mode in optical frequency conversion systems. *Physics Letters A*, 239:59–64(6), 23 February 1998.

[15] L. Yang, A. M. Zhabotinsky, and I. R. Epstein. Stable squares and other oscillatory Turing patterns in a reaction-diffusion model. *Physical Review Letters*, 92(19):198303–+, May 2004.

[16] Vladimir K. Vanag and Irving R. Epstein. Stationary and oscillatory localized patterns, and subcritical bifurcations. *Phys. Rev. Lett.*, 92(12):128301, Mar 2004.

[17] A. Yochelis, C. Elphick, A. Hagberg, and E. Meron. Frequency locking in extended systems: The impact of a Turing mode. *Europhysics Letters*, 69(2):170–176, Jan 2005.

[18] D. G. Miguez, R. A. Satnoianu, and A. P. Munuzuri. Experimental steady pattern formation in reaction-diffusion-advection systems. *Phys. Rev. E*, 73:025201, 2006.

[19] A. Lampert and E. Meron. Localized structures as spatial hosts for unstable modes. *EPL (Europhysics Letters)*, 78(1):14002 (5pp), 2007.

[20] M.I. Weinstein and J. Xin. Dynamic stability of vortex solutions of Ginzburg-Landau and nonlinear Schrodinger equations. *Communications in Mathematical Physics*, 180(2):389–428, OCT 1996.

[21] FH Lin and JX Xin. On the dynamical law of the Ginzburg-Landau vortices on the plane. *Communications in Mathematical Physics*, 52(10):1189–1212, OCT 1999.

[22] Igor Aranson and Lorenz Kramer. The world of the complex Ginzburg-Landau equation. *Reviews of Modern Physics*, 74:99, 2002.

[23] W. van Saarloos. The complex Ginzburg-Landau equation for beginners. *Proceedings of the Santa Fe workshop on 'Spatio-Temporal Patterns in Nonequilibrium Complex Systems'*, pages 19–31, 1994.

[24] W. van Saarloos and P. C. Hohenberg. Fronts, pulses, sources and sinks in generalized complex Ginzburg-Landau equations. *Physica D Nonlinear Phenomena*, 56:303–367, June 1992.

[25] Tornkvist O. and Schroder E. Vortex dynamics in dissipative systems. *Physical Review Letters*, 78:1908, 1997.

[26] M. Stich. *Target patterns and pacemakers in reaction-diffusion systems.* PhD thesis, Technische Universität Berlin, 2003.

[27] H. Chaté and P. Manneville. Phase diagram of the two-dimensional complex Ginzburg-Landau equation. *Physica A Statistical Mechanics and its Applications*, February 1996.

[28] P Coullet and J Lega. Defect-Mediated Turbulence in Wave Patterns. *Europhysis Letters*, 7(6):511–516, NOV 15 1988.

[29] Bradley Marts, Aric Hagberg, Ehud Meron, and Anna L. Lin. Bloch-front turbulence in a periodically forced belousov-zhabotinsky reaction. *Phys. Rev. Lett.*, 93(10):108305, Sep 2004.

[30] Fagen Xie, Dongzhu Xie, and James N. Weiss. Inwardly rotating spiral wave breakup in oscillatory reaction-diffusion media. *Physical Review E*, 74(2, Part 2), AUG 2006.

[31] Martin Falcke Markus Bär and Michal Or-Guil. *Mechanisms of spiral breakup in chemical and biological reaction-diffusion models*, pages 326–348. Springer Berlin / Heidelberg, 1999.

[32] Haye Hinrichsen. Nonequilibrium critical phenomena and phase transitions into absorbing states. *Advances in Physics*, 49:815, 2000.

[33] William H. Press, Saul A. Teukolsky, William T. Vetterling, and Brian P. Flannery. *Numerical Recipes in C: The Art of Scientific Computing.* Cambridge University Press, New York, NY, USA, 1992.

[34] I. Berenstein, M. Dolnik, A.M. Zhabotinsky, and I.R. Epstein. Spatial periodic perturbation of Turing pattern development using a striped mask. *Journal of Physical Chemistry A*, 107(22):4428–4435, JUN 5 2003.

[35] D. Balasubramanian and G. A. Rodley. Incorporation of chemical oscillators into organized surfactant assemblies. *Journal of Physical Chemistry*, 92:5995–5998, 1988.

[36] V.K. Vanag and I. Hanazaki. Frequency-Multiplying Bifurcation in the Oscillatory Belousov-Zhabotinskii Reaction Proceeding in Interacting Water Droplets of the Reverse Microemulsion of the Aerosol OT in Octane. *Journal of Physical Chemistry*, 99(18):6944–6950, MAY 4 1995.

[37] V.K. Vanag and I.R. Epstein. Pattern formation in a tunable medium: The Belousov-Zhabotinsky reaction in an aerosol OT microemulsion. *Physical Review Letters*, 8722(22), NOV 26 2001.